Supporting Information for

# Syntheses, crystal structures and properties of metal-organic rotaxane frameworks with cucurbit[6]uril

Jun Liang,[a,b] Xue-Song Wu,[a] Xin-Long Wang,*[a] Chao Qin,[a] Kui-Zhan Shao,[a] Zhong-Min Su,*[a] and Rong Cao[b]

[a] Institute of Functional Material Chemistry, Key Lab of Polyoxometalate Science of Ministry of Education, Faculty of Chemistry, Northeast Normal University, Changchun 130024, P. R. China. Fax:+86 431-85684009; E-mail: wangxl824@nenu.edu.cn; zmsu@nenu.edu.cn

[b] Department of Chemistry, College of Chemistry and Chemical Engineering, Xiamen University, Xiamen 361005，P. R. China

**CONTENTS**

**Section 1 Preparation of composites**

For **X:Eu** (X=**1, 3, 4, 5, CB[6]HP**).

In our initial screening study, crystals of compound **n** (n= **1**, **3**, **4**, **5**) and hexagonal CB[6] crystals were separately soaked in ethanol solutions containing 0.3 M nitrate salts of $Eu^{3+}$ for three days to prepare the composites as below:

5 50 mg crystals of freshly prepared compound n (n= **1, 3, 4, 5**) and CB[6]s were separately soaked in ethanol solutions containing nitrate salts of $Eu^{3+}$ (0.6 mmol in 2 ml ethanol) for three days before being taken out and washed gently with 20 ml distilled water to remove free europium salt on crystal surfaces, then dried in air for three days. These composites were marked as **X:Eu** (X=**1, 3, 4, 5, CB[6]HP**) for simplification. Dilute ethanol solutions (0.1 M or 0.2 M) of corresponding Ln salts wouldn't facilitate the post-synthetic surface modifications and would usually take 10 more time, leading to not so good composites.

For **3:Ln** (Ln= $Sm^{3+}$, $Eu^{3+}$, $Tb^{3+}$, $Dy^{3+}$).

**3:Ln** (Ln= $Sm^{3+}$, $Eu^{3+}$, $Tb^{3+}$ or $Dy^{3+}$) sample was prepared by immersing freshly prepared compound **3** (100 mg) in ethanol solutions containing lanthanide nitrates of Ln ( $Sm^{3+}$, $Eu^{3+}$, $Tb^{3+}$ or $Dy^{3+}$) (0.6 mmol in 2 ml ethanol). After 3 days of soakage, respectively, the crystals were taken out of solution and washed with distilled water to remove free 15 lanthanide cations on the surfaces. The 'antenna effect' of these compounds remained when composites were left in the air for months.
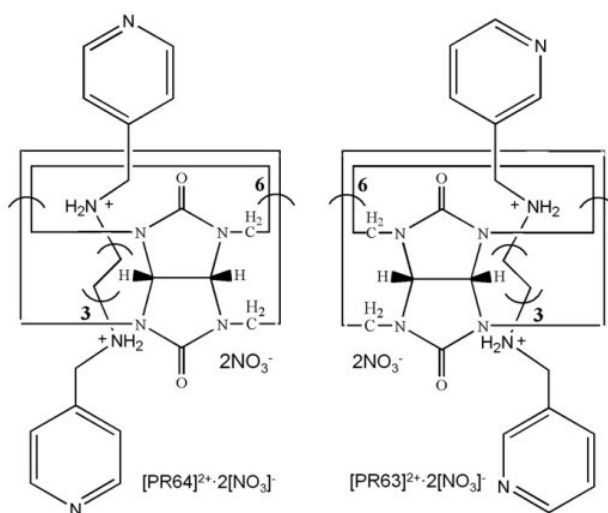


20 Fig. S1. Chemical views of pseudorotaxanes [PR64]$^{2+}$·2[NO$_3$]$^-$ and [PR63]$^{2+}$·2[NO$_3$]$^-$.[1]

25

30

## Section 2 Supplementary data of compounds 1-5

**Table S1.** Crystal Data and Structure Refinement for **1–5**

| Compound | **1** | **2** | **3** | **4** | **5** |
|---|---|---|---|---|---|
| Empirical formula | $C_{78}H_{106}N_{28}O_{39}Cd_2$ | $C_{41}H_{46}N_{14}O_{13}CdCl$ | $C_{35}H_{40}N_{14}O_{13}ZnCl$ | $C_{86}H_{122}N_{28}O_{49}Cd_3$ | $C_{144}H_{164}N_{58}O_{72}Cd_5$ |
| $M$ | 2284.70 | 1090.77 | 965.63 | 2669.31 | 4421.32 |
| $T$/K | 298(2) | 298(2) | 298(2) | 298(2) | 298(2) |
| Crystal system | Monoclinic | Monoclinic | Monoclinic | Tetragonal | Triclinic |
| Space group | $C2/c$ | $P2_1/c$ | $P2_1/c$ | $P4_12_12$ | $P\text{-}1$ |
| $a$/Å | 18.185 (4) | 11.511(5) | 14.218(5) | 16.364(5) | 15.482(5) |
| $b$/Å | 28.670(6) | 29.125(5) | 16.432(5) | 16.364(5) | 16.212(5) |
| $c$/Å | 20.572(5) | 14.591(5) | 17.815(5) | 41.797(5) | 19.631(5) |
| $\alpha$/° | 90 | 90. | 90 | 90 | 93.931(5) |
| $\beta$/° | 108.003(7) | 103.215(5) | 104.505(5) | 90 | 103.836(5) |
| $\gamma$/° | 90 | 90 | 90 | 90 | 106.406(5) |
| $V$/Å$^3$ | 10200(4) | 4762(3) | 4029(2) | 11192(7) | 4540(2) |
| $Z$ | 4 | 4 | 4 | 4 | 1 |
| $D_c$/Mg m$^{-3}$ | 1.488 | 1.521 | 1.592 | 1.584 | 1.617 |
| Measured reflections | 26311 | 27384 | 20478 | 58067 | 23602 |
| Independent reflections | 8963 | 8383 | 7080 | 9862 | 15803 |
| $R_{int}$ | 0.1246 | 0.1067 | 0.0624 | 0.0652 | 0.0704 |
| $R_1(I > 2\sigma(I))$ [a] | 0.0892 | 0.0796 | 0.0555 | 0.0718 | 0.0884 |
| $wR_2$ (all data) [a] | 0.2913 | 0.2651 | 0.1587 | 0.2111 | 0.2844 |
| Goodness-of-fit on $F^2$ | 1.029 | 1.019 | 1.018 | 1.065 | 1.018 |

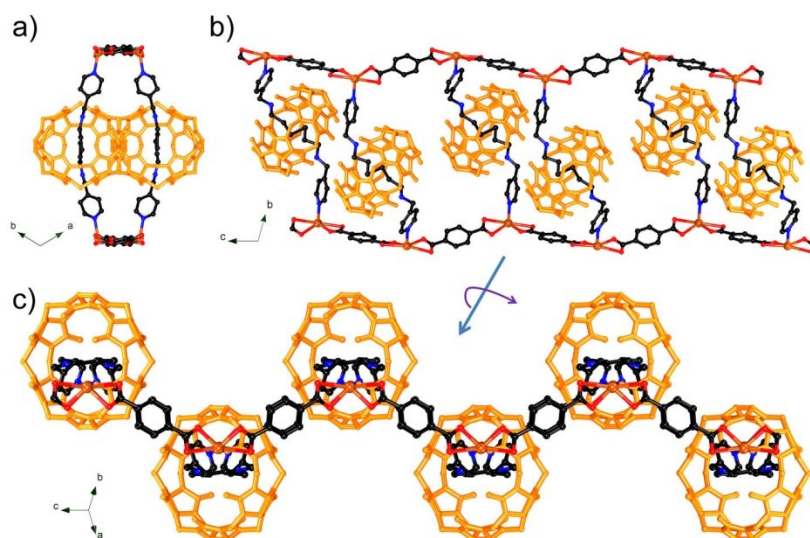[a] $R_1 = \Sigma||F_o| - |F_c||/\Sigma|F_o|$. [b] $wR_2 = |\Sigma w(|F_o|^2 - |F_c|^2)|/\Sigma|w(F_o^2)^2|^{1/2}$

Fig. S2. Perspective views of adjacent pillaring ligands [**PR64**]$^{2+}$ in one framework of compound **1**. Color code: C, black; N, blue; O, red; Cd, brown; CB[6], orange.
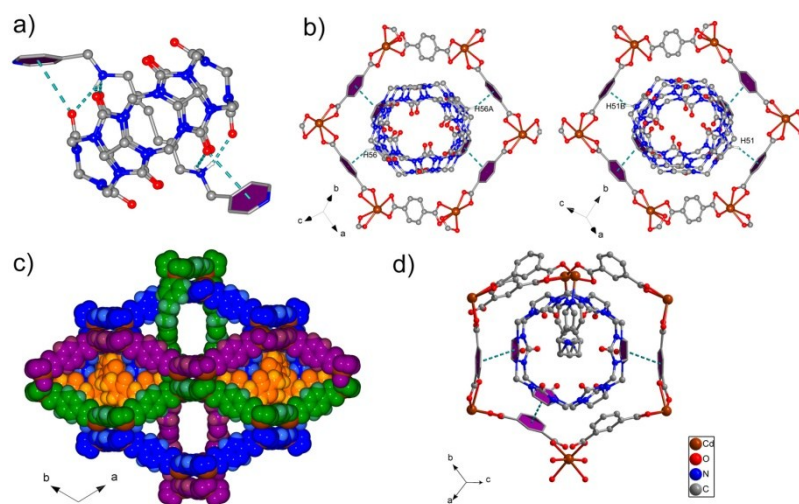


Fig. S3. Ball-and-stick representations of a) intra-rotaxanic $\pi\cdots\pi$ interactions (3.610 Å) in [PR64]; b) C-H$\cdots\pi$ (2.731 Å) as well as weak $\pi\cdots\pi$ interactions (3.71 Å) around [BDC-Cd]$_6$ units in compound **1**. c) Space-filling view of all CB[6]s in one net are well arrayed between two layers from other two interpenetrating nets (violet and green) in compound **1**. CB[6]s (orange) are shown only in one net (blue). d) The $\pi\cdots\pi$ stacking interactions (average distance 3.936 Å) between *m*-BDC$^{2-}$ ligands and rings of CB[6] in compound **4**. Note: Dashed cyan lines represent C-H$\cdots\pi$ or $\pi\cdots\pi$ interactions.
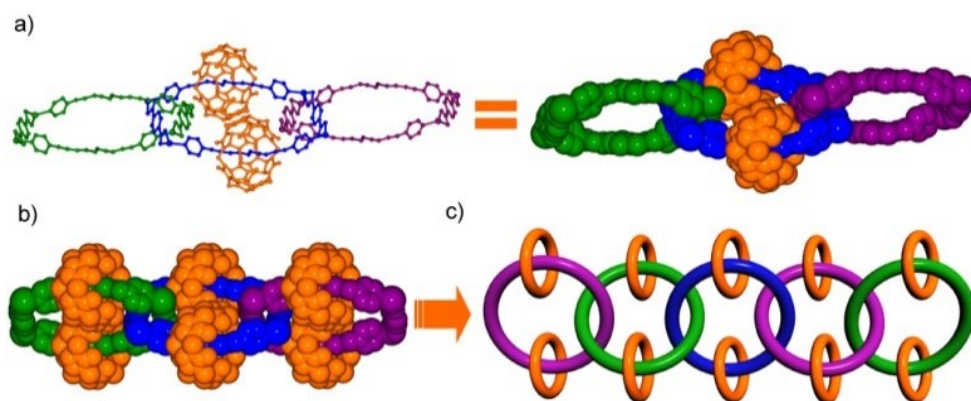
Fig. S4. a) Chemical view of the in-separate MN[5]s composed of two CB[6]s and three [Cd$_2$·BDC·C6N4]$_2$ loops from three separate nets of MORF-**1**. b) Space-filling and c) schematic views of the resulted novel 1D 'polycatenanes' in **1**.



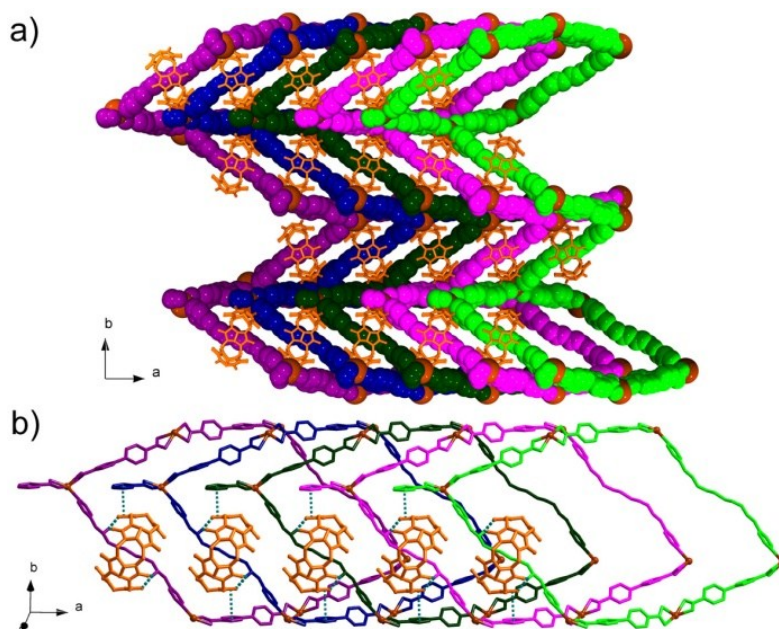Fig. S5. a) The tiling array of 3D supramolecular architectures as viewed along the a axis and b) the π⋯π interactions (3.69 Å) between CB[6]s and BPDC struts of adjacent layers in compound **2**. Dashed lines: hydrogen bonds or π⋯π interactions.
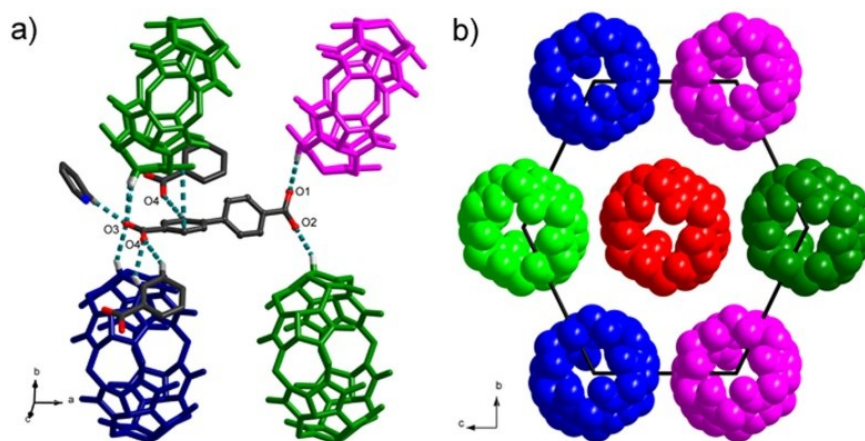
Fig. S6. a) The π···π interactions (3.69 Å) as well as hydrogen bonds (2.387-2.698 Å) around each BPDC ligand in compound **2**. CB[6]s from other three layers are in purple, green and blue, respectively. b) Schematic view of CB[6] (red) in one net is coplanar with six CB[6]s from four other frameworks along the a axis. Dashed line: hydrogen bonds or π···π interactions.
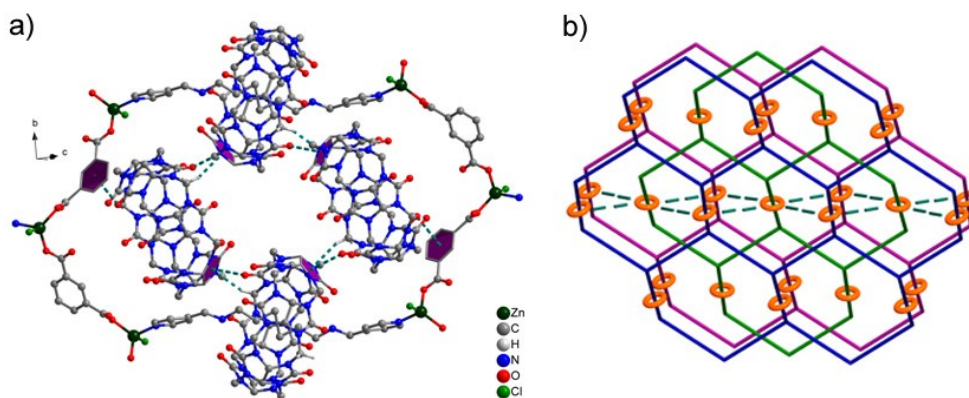


Fig. S7. a) Ball-and-stick representation of the basic supra-molecular tetramer of CB[6]s from three nets based on C-H···π (average 2.78 Å) and π···π interactions (from 3.34-3.50 Å) in compound **3**. (b) The schematic illustration of three layers closely stacked in an inlaid manner. Dashed cyan lines represent C-H···π and π···π interactions.
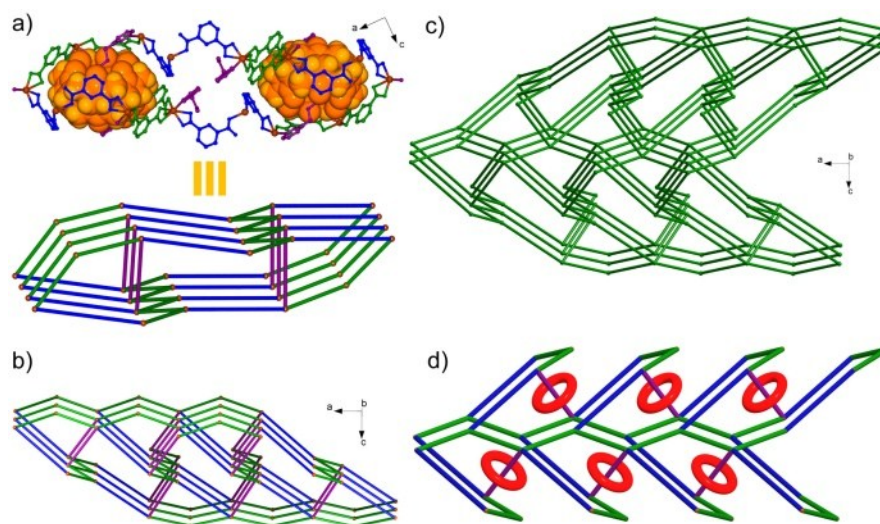
Fig. S8. a) Chemical and b) schematic view of basic 1D elliptic cylindrical MORFs in compound **4**. c) The topological presentation of *snw* network of compound **4**. d) A catoon depiction of the 3D branched MORFs in compound **4**. Color code: green: *m*-BDC; blue: [Cd(*m*-BDC$^{2-}$)$_2$·4Ow]; violet rod: [**PR63**]$^{2+}$; orange or red: CB[6]. Hydrogen atoms are omitted.
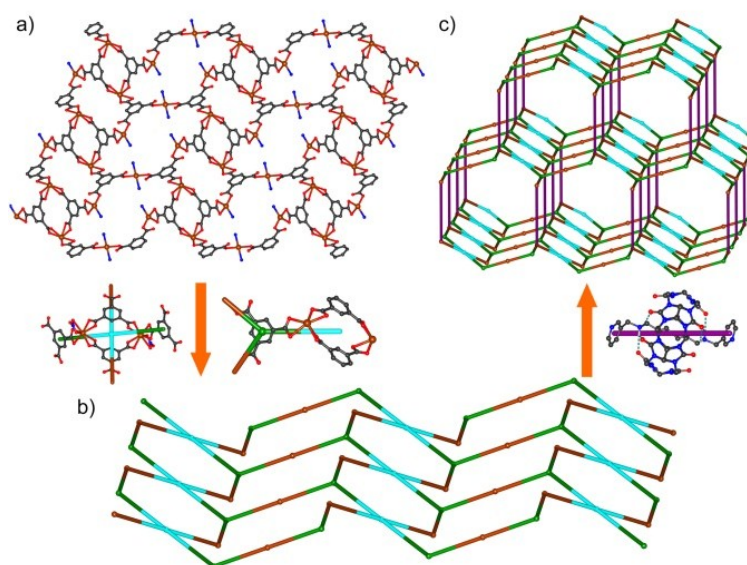


Fig. S9. a) Ball-and-stick view of the 2D wavy layer formed by 16-membered rings, 32-membered rings and 48-membered rings in compound **5**. b) The simplified 3, 4-c wavy net. c) Schematic view of the virtual single 3, 3, 4-c framework in the 3D MORFs. Note: Hydrogen atoms are omitted for clarity.
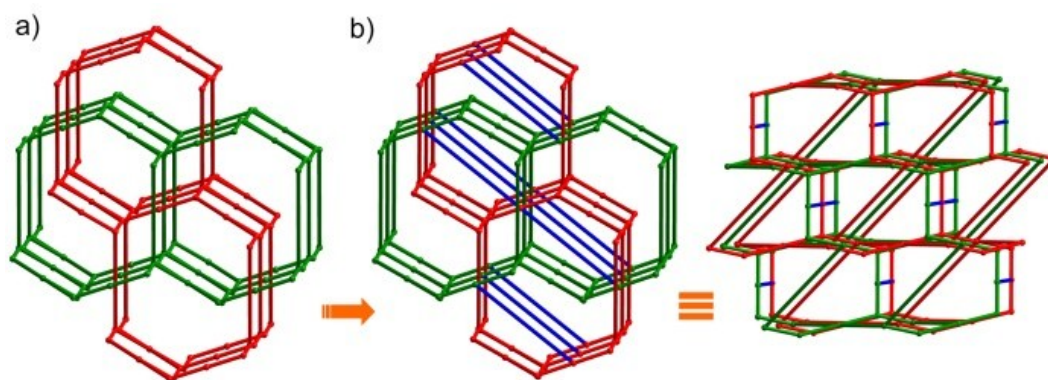
Fig. S10. Topological illustration of how a) two identical interpenetrating 3, 3, 4-c nets are merged into b) one non-interpenetrating 3, 3, 4, 4-c nets in compound **5**.
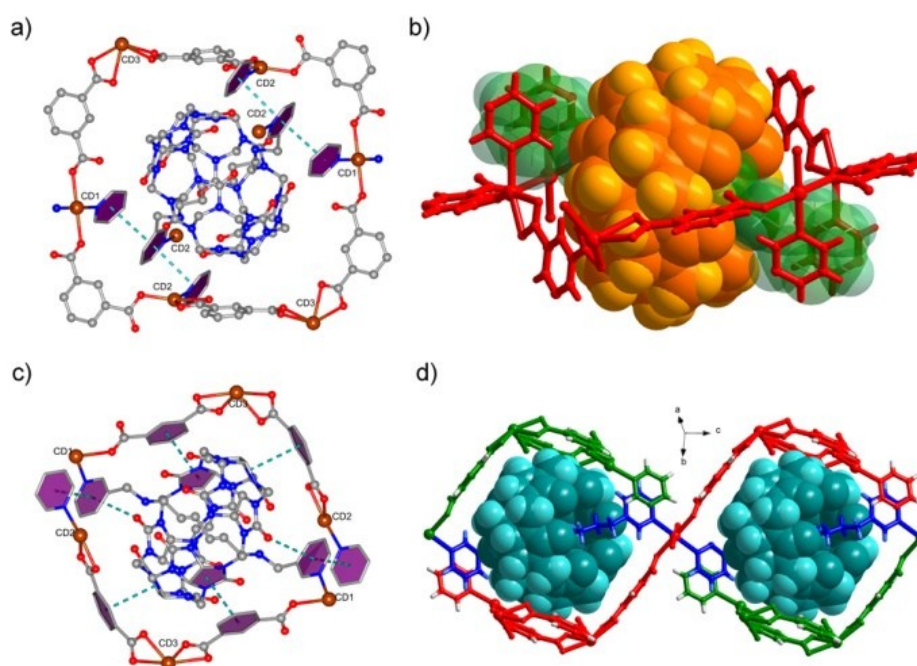


Fig. S11. Ball-and-stick representations of a) the 3-fold $\pi\cdots\pi$ interactions (3.68 Å and 3.90 Å) between $\alpha$-[**PR63**]$^{2+}$ and $\beta$-[**PR63**]$^{2+}$; c) intra- and outer $\pi\cdots\pi$ interactions (3.258 Å , 3.628-3.750 Å, respectively) of $\beta$-[**PR63**]$^{2+}$ in compound **5**. The chemical environments of b) $\alpha$-[**PR63**]$^{2+}$ and d) $\beta$-[**PR63**]$^{2+}$. Hydrogen atoms are omitted. Color code: gray: C; blue: N; red: O; brown: Cd; orange or teal: CB[6]. Note: Dashed cyan lines represent $\pi\cdots\pi$ interactions.

**Table S2. Structure parameters for pseudorotaxanes in MORFs**

| Pseudorotaxane | Compound | Distance($d$, Å) | Dihedral angles ($\delta$, °) |
|---|---|---|---|
| $\alpha$-[PR64] | {Ag.[PR64].[NO$_3$]$^-$.xH$_2$O}[1c] | 15.10 | 0 |
| $\beta$-[PR64] | | 13.72 | 0 |
| [PR64]$^{2+}$ | **1** [Cd$_2$(BDC)$_3$(PR64)]·9H$_2$O | 14.58 | 53 |
| | **2** [Cd(BPDC)(PR64)$_{0.5}$Cl]·2H$_2$O | 15.54 | 0 |
| | **3** [Zn(PR64)$_{0.5}$(m-BDC)Cl]·3H$_2$O | 15.23 | 0 |
| [PR63]$^{2+}$ | [Ag(H2**C6N3**)(CB[6])](NO$_3$)$_3$. 8H$_2$O[1a] | 15.15 | 0 |
| [PR63]$^{2+}$ | **4**[Cd$_{1.5}$(m-BDC)$_2$(PR63)$_{0.5}$(H$_2$O)$_2$]·11H$_2$O | 13.64 | 8.6 |
| $\alpha$-[PR63]$^{2+}$ | **5**[Cd$_{2.5}$(BTC)$_2$(PR63)(NO$_3^-$)(H$_2$O)$_3$]·11H$_2$O | 15.65 | 0 |
| $\beta$-[PR63]$^{2+}$ | | 15 | 0 |

Note: $d$ and $\delta$ are the centroid distances and the dihedral angles between two terminal pyridine groups of certain pseudorotaxanes in corresponding compound.



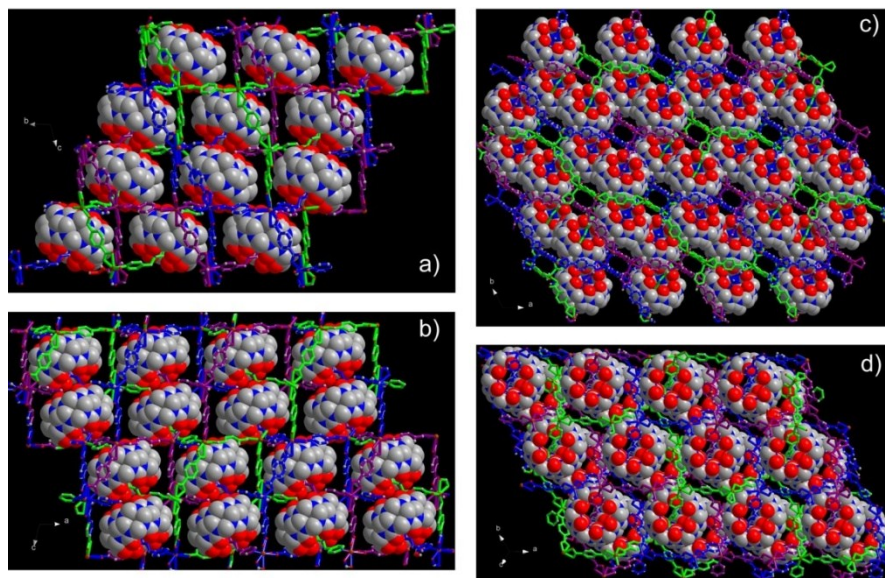Fig. S12. Perspective views of CB[6]s in the frameworks of compound **1**. Hydrogen atoms are omitted.
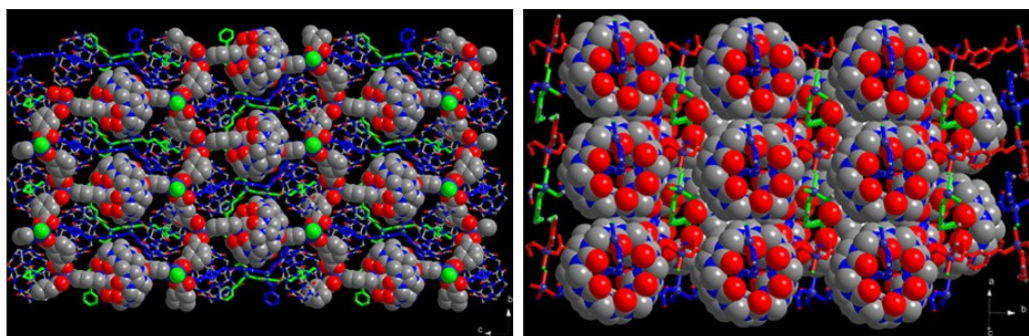
Fig. S13. Perspective views of CB[6]s in the frameworks of compound **3**. Hydrogen atoms are omitted.
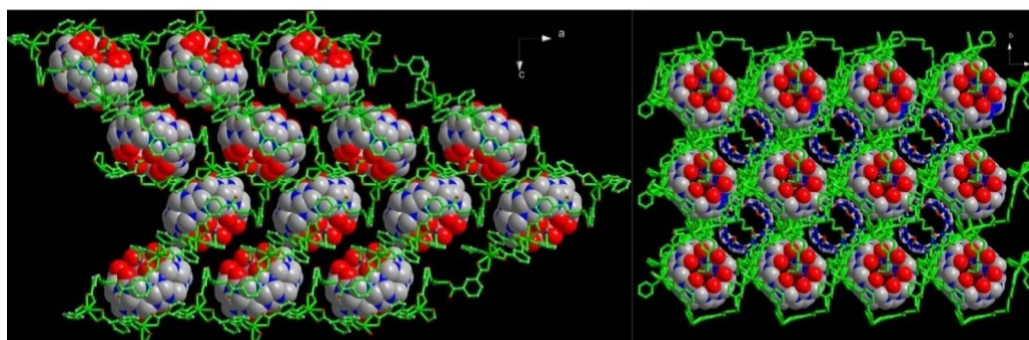


Fig. S14. Perspective views of CB[6]s in the branched framework of compound **4**. Hydrogen atoms are omitted.
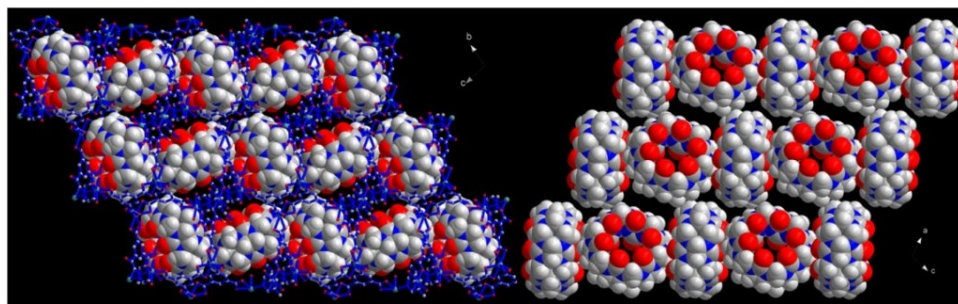


Fig. S15. Perspective views of CB[6]s in compound **5** a) with and b) without the metal-organic frameworks.
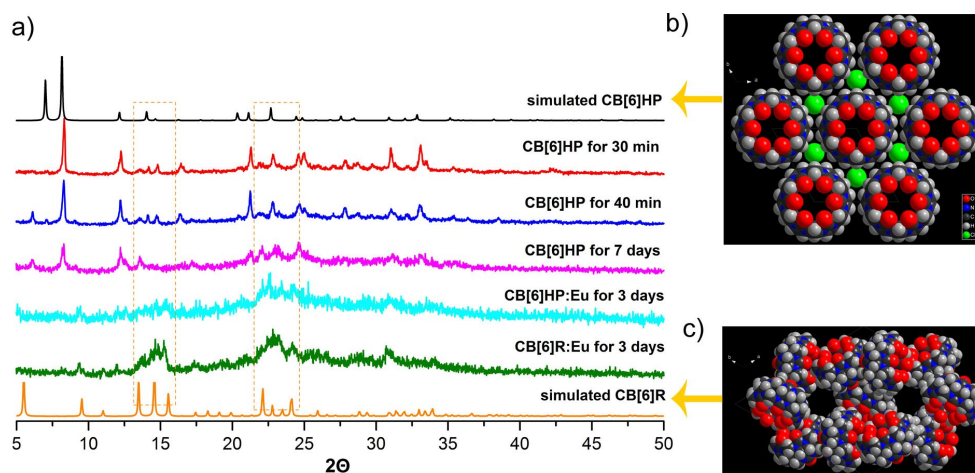
Fig. S16. a) PXRD patterns of composites **CB[6]HP:Eu** and **CB[6]R:Eu** derived from b) hexagonal CB[6] *P6/ mmm* crystals and c) the CB[6] *R-3* crystals. These data are compared to data simulated from single-crystal diffraction data of **CB[6]HP** synthesized here and **CB[6]R** from literature[2].

Many efforts has been done to investigate this process and it proved that the fresh or dried **CB[6]HP** crystals couldn't retain its original crystallinity after being soaked in ethanol for a few days. Actually, semi-crystalline **CB[6]HP:Eu** could be observed in most cases (whether being washed by water or not). **CB[6]R** also proved to be unable for sensing $Eu^{3+}$ ions under the same conditions.

**Section 3 Supplementary Physical Characterizations**
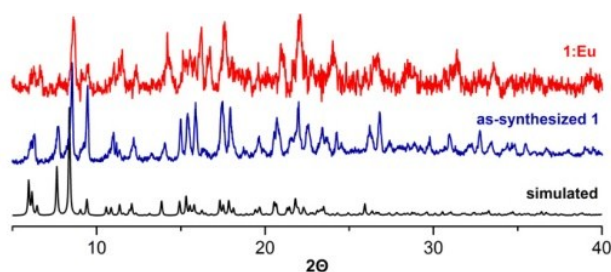


Fig. S17. PXRD patterns for compound **1** and **1:Eu**. Black (simulated spectra from single crystal data).
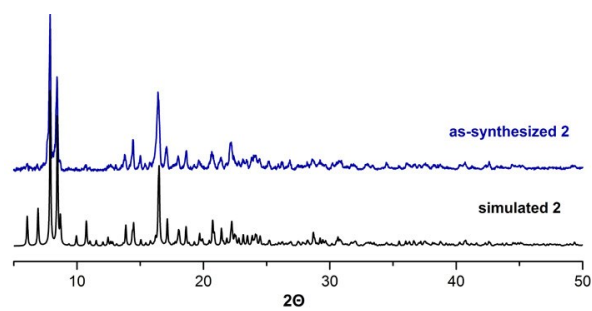
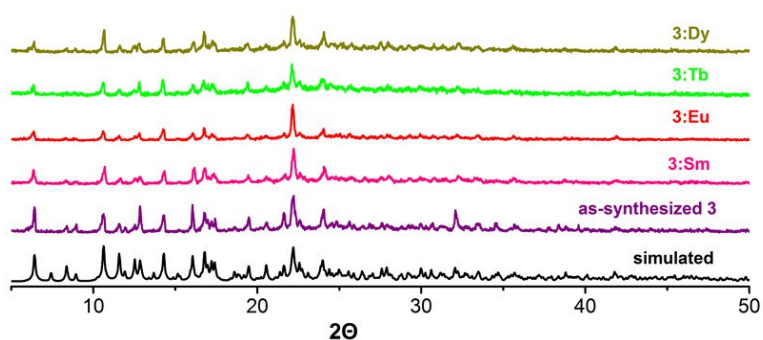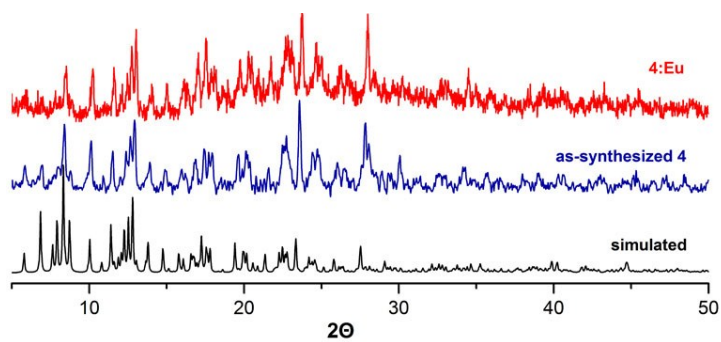Fig. S18. PXRD patterns for compound **2** and simulated spectra of **2** from single crystal data



Fig. S19. PXRD patterns for compound **3** and **3:Ln** (Ln= $Sm^{3+}$, $Eu^{3+}$, $Tb^{3+}$, $Dy^{3+}$). Black (simulated spectra from single crystal data).



Fig. S20. PXRD patterns for compound **4** and **4:Eu**. Black (simulated spectra from single crystal data).
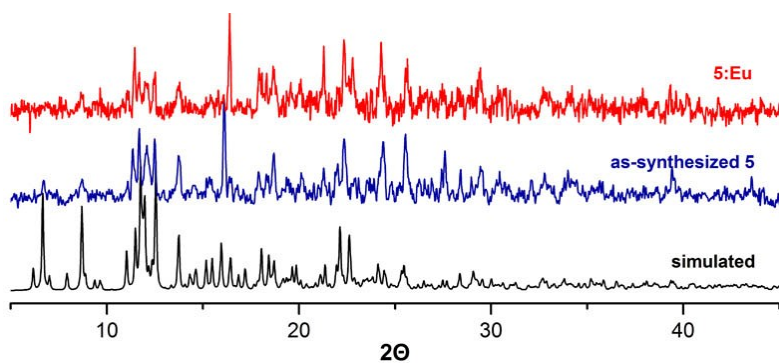
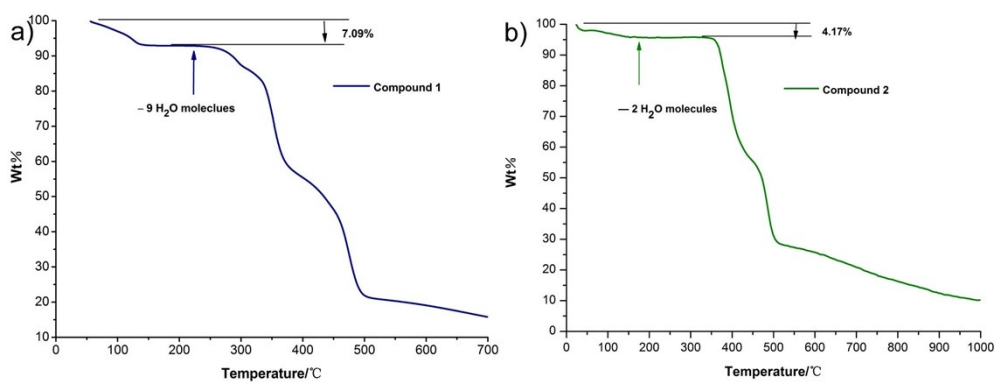Fig. S21. PXRD patterns for compound **5** and **5:Eu**. Black (simulated spectra from single crystal data).



Fig. S22. Thermal gravimetric analysis (TGA) curves for as-synthesized a) compound **1** and b) compound **2.**
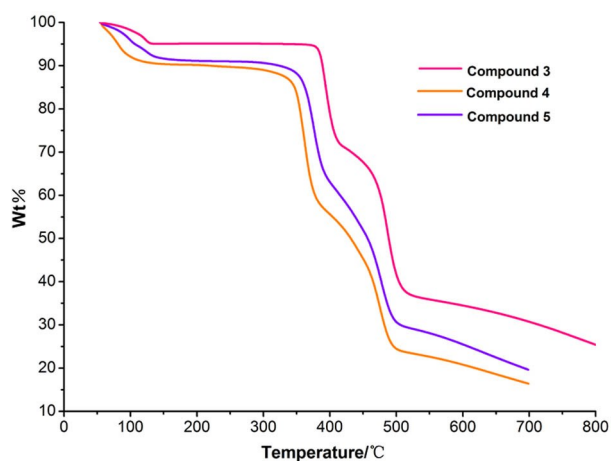


Fig. S23. Thermal gravimetric analysis (TGA) curves for as-synthesized compound **3**, **4** and **5**.
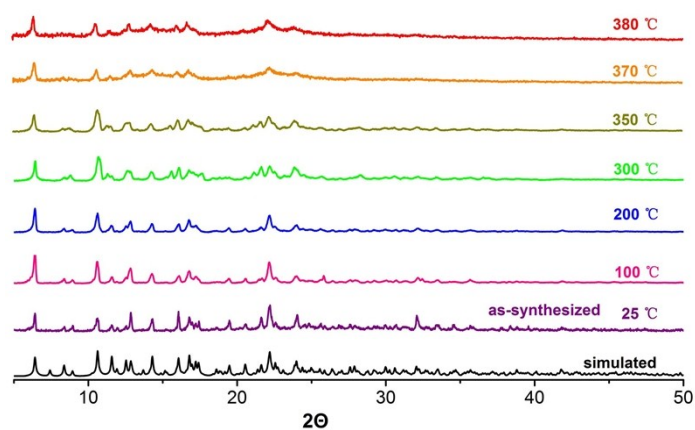
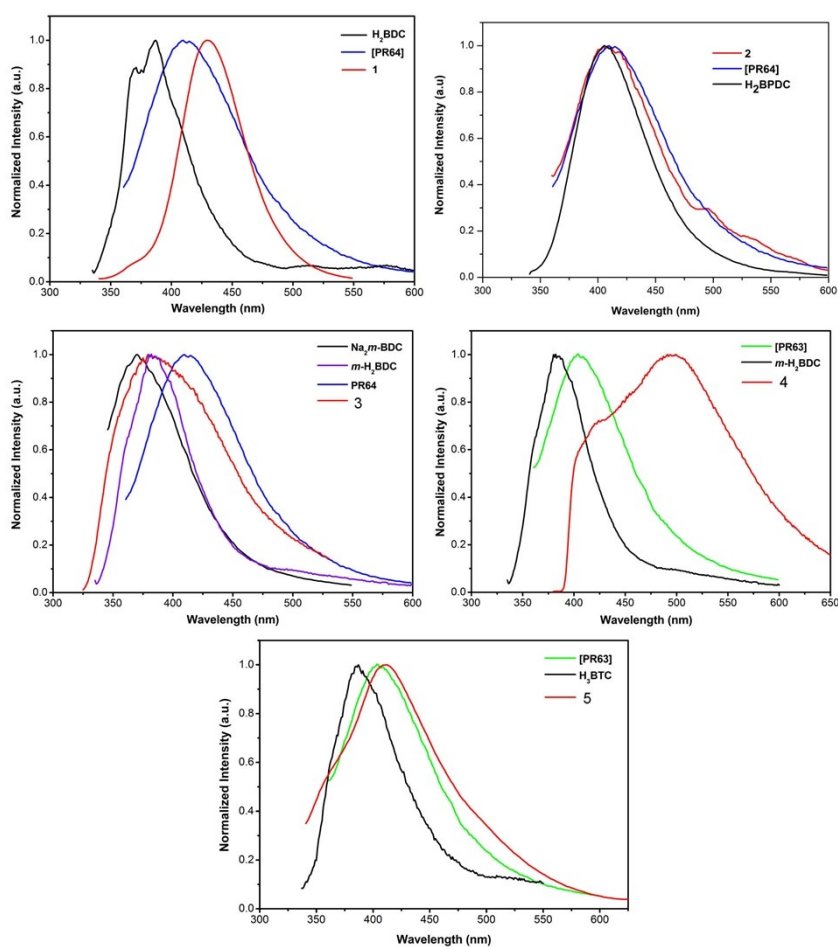Fig. S24. Variable temperature PXRD data for **3**.



Fig. S25. Emission spectra of compound **1**, **2**, **3**, **4**, **5** and related organic linkers in the solid state at room temperature. Although the emissions of $[PR64]^{2+}.2[NO_3]^-$ and $[PR63]^{2+}.2[NO_3]^-$ are very weak, they're normalized for comparison.

Table S3. Wavelengths λ[nm] of the emission maxima and excitation of compound **1**, **2**, **3**, **4**, **5** and related ligands.

| MORF: | **1** | **2** | **3** | **4** | **5** |
|---|---|---|---|---|---|
| $\lambda_{em}$ | 429 | 410 | 383 | 494 | 412 |
| $\lambda_{ex}$ | 333 | 340 | 312 | 344 | 320 |

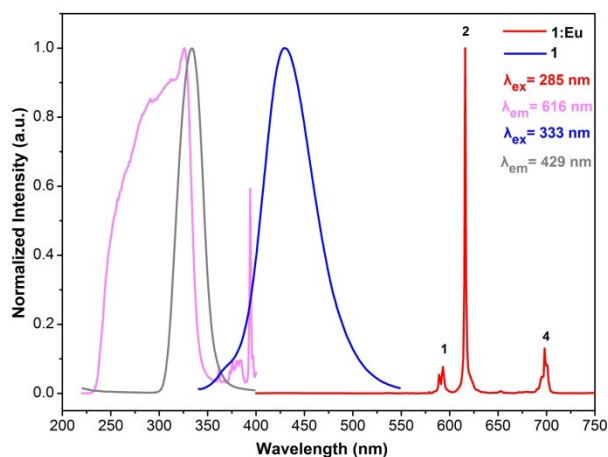| Ligands: | $H_2BDC$ | $H_2BPDC$ | $m$-$H_2BDC$ | $H_3BTC$ | $[PR64]^{2+}.2[NO_3]^-$ | $[PR63].2[NO_3]^-$ | $CB[6]^{[3]}$ |
|---|---|---|---|---|---|---|---|
| $\lambda_{em}$ | 387 | 408 | 380 | 387 | 410 | 404 | 439 |
| $\lambda_{ex}$ | 330 | 320 | 333 | 322 | 341 | 337 | 371 |



Fig. S26. Photoluminescence excitation (PLE) and emission spectra of crystals of **1:Eu** and compound **1** measured at room temperature. Emission bands 1, 2, 4 correspond to transitions $^5D_0\rightarrow{}^7F_J$, J =1, 2, 4. 593, 616, 699 nm. A broad PLE band at~280 nm corresponds to absorption of ligands. Almost no signature of the $^5D_0\rightarrow{}^7F_0$ transition and the notably narrow bands are observed in the emission spectra of **1:Eu**, suggesting a high local symmetry for the Eu ions.
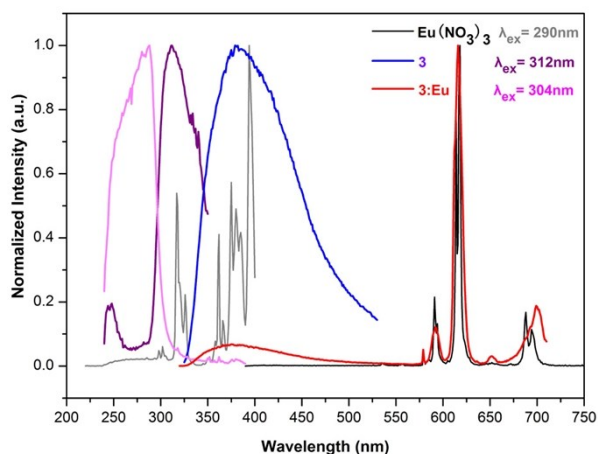
Fig. S27. The comparison of photoluminescence excitation (PLE) and emission spectra of crystals of **3:Eu** (red), compound **3** (blue) and $Eu(NO_3)_3.6H_2O$ (black), respectively. A broad PLE band at~280 nm corresponds to absorption of ligands.
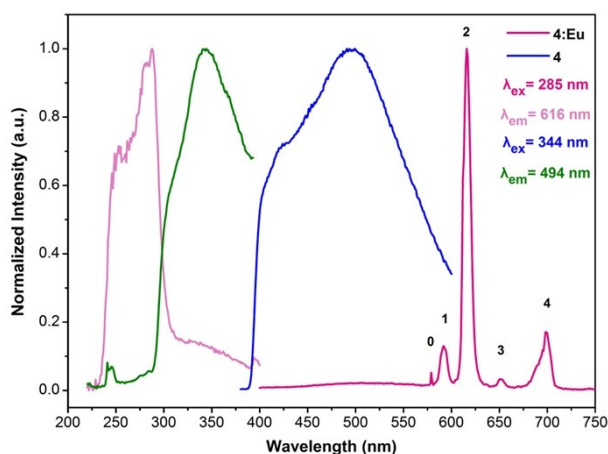


Fig. S28. Photoluminescence excitation (PLE) and emission spectra of crystals of **4:Eu** and compound **4**. Emission bands 0-4 correspond to transitions $^5D_0 \rightarrow {}^7F_J$, J =0, 1, 2, 3, 4. 579, 593, 617, 652, 699 nm. A broad PLE band at~280 nm corresponds to absorption of ligands.
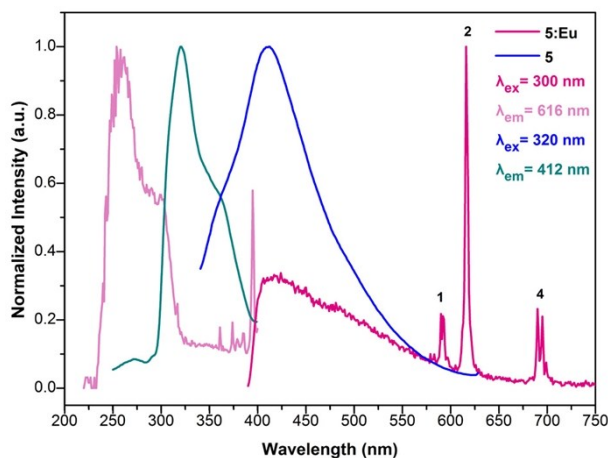


Fig. S29. Photoluminescence excitation (PLE) and emission spectra of crystals of **5:Eu** and compound **5**. Emission bands 1, 2, 4 correspond to transitions $^5D_0 \rightarrow {}^7F_J$, J =1, 2, 4. 590, 616, 690 nm.
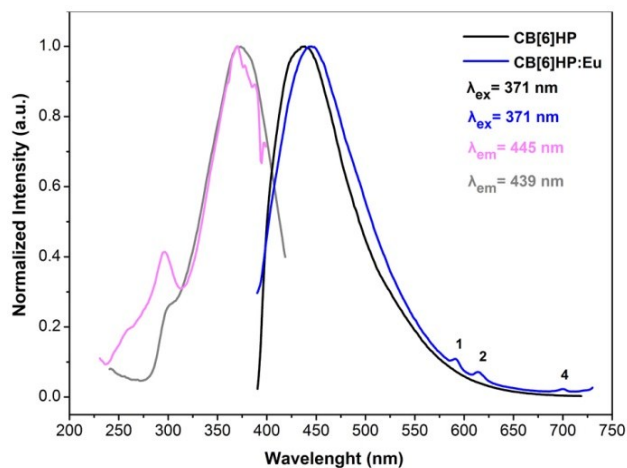
Fig. S30. The comparison of photoluminescence excitation (PLE) and emission spectra of crystals of **CB[6]HP:Eu** (magenta and blue) and **CB[6]HP** (gray and black), respectively. Weak emission bands 1-4 correspond to transitions $^5D_0 \rightarrow {}^7F_J$, J =1, 2, 4 (591, 614, 700 nm). The enhanced PLE band at~280 nm corresponds to absorption of the CB[6] ligands. This means that only traces of europium ions could be sensitized on the surfaces of cucurbit[6]uril crystals efficiently, but this observation strongly supports the possible coordination interactions between lanthanide ions and carbonyl groups on the surfaces of compound **1**, **3-5**.
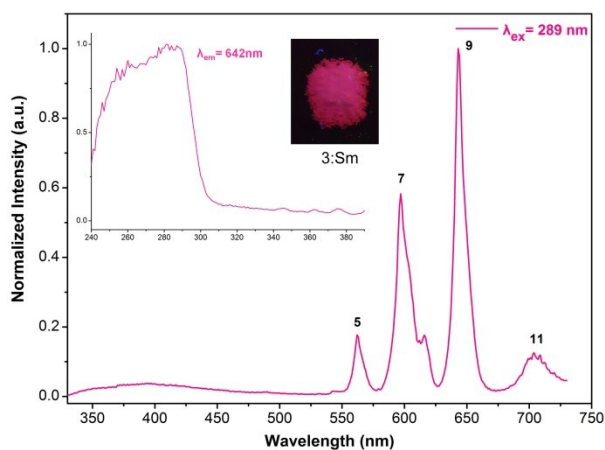


Fig. S31. Photoluminescence excitation (PLE) and emission spectra of crystals of **3:Sm** measured at room temperature. The insets are the optical photographs of **3:Sm** excited under 254 nm ultraviolet lamps. Emission bands 5, 7, 9, 11 correspond to transitions $^4G_{5/2} \rightarrow {}^6H_{J/2}$, J=5, 7, 9, 11 (562, 597, 643,704 nm).
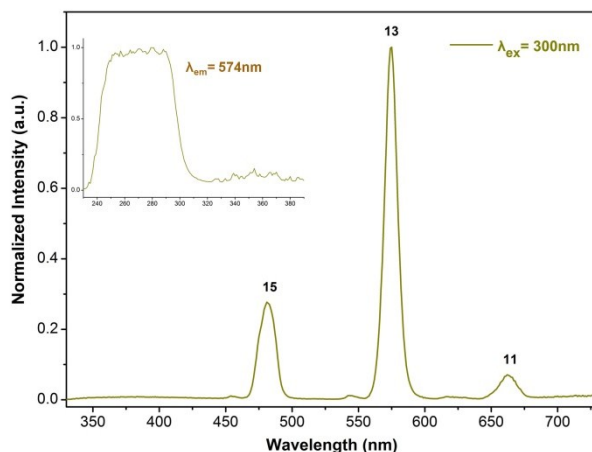
Fig. S32. Photoluminescence excitation (PLE) and emission spectra of crystals of **3:Dy** measured at room temperature. The insets are the optical photographs of **3:Dy** excited under 254 nm ultraviolet lamps. Emission bands 15, 13, 11 correspond to transitions $^4F_{9/2} \rightarrow {}^6H_{J/2}$, J =15, 13, 11 (481, 574, 662 nm).

**UV-vis spectra of 3:Ln.**

The two adsorption peaks (about 264 nm and 285 nm) are ascribed to the $\pi \rightarrow \pi^*$ and $n \rightarrow \pi^*$ transitions of C=O. The adsorption intensities of all five composites are higher than that of CB[6] and different from that of compound **3**, which might be the result of coordination interactions between Ln ions and carboxylic groups on the surfaces of **3**.
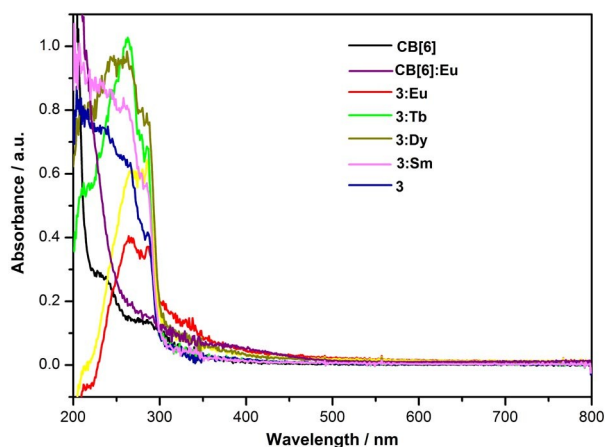


Fig. S33. UV-vis adsorption of CB[6], compound **3** and **3:Ln** (Ln = $Eu^{3+}$, $Tb^{3+}$, $Sm^{3+}$, $Dy^{3+}$).
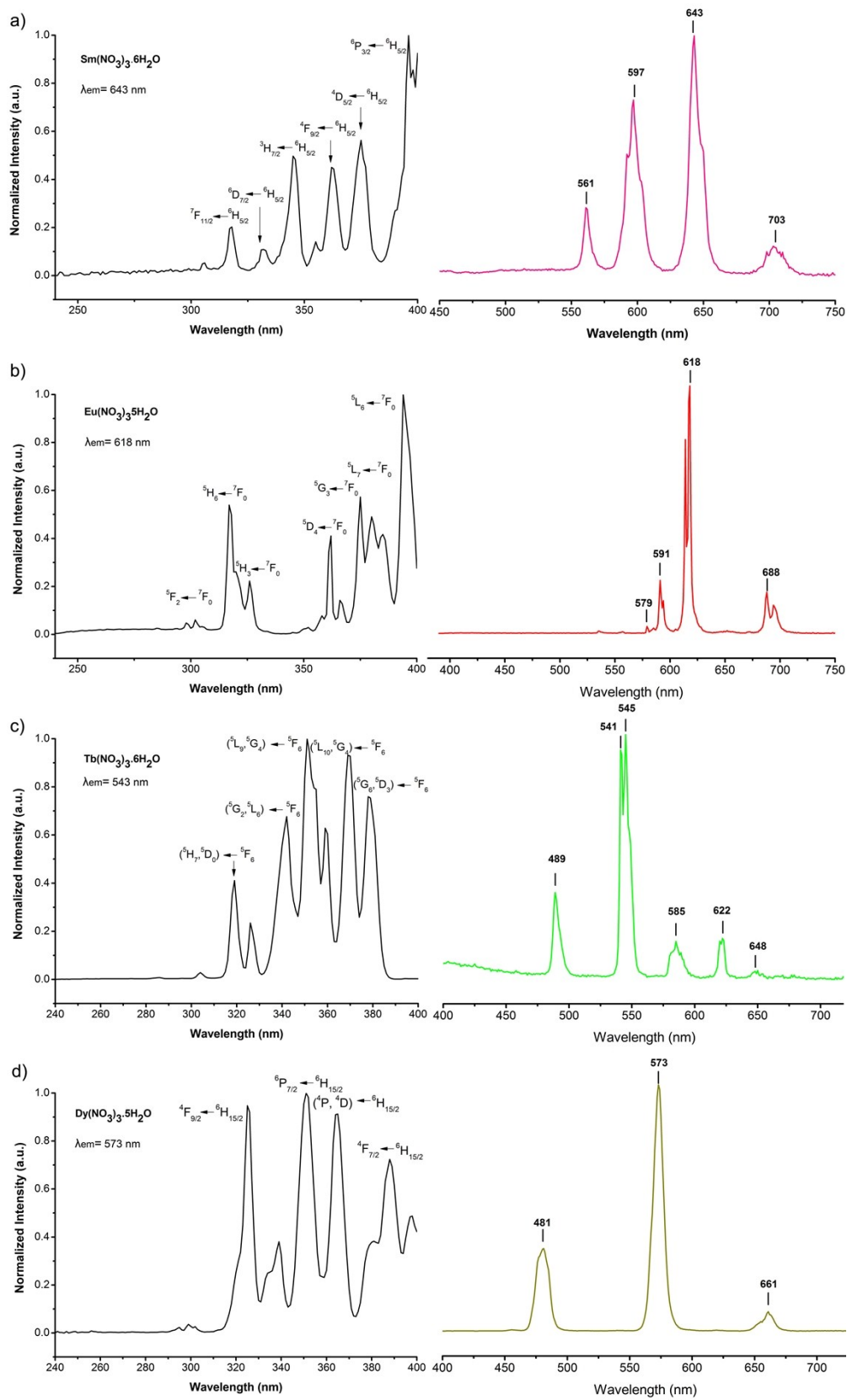
Fig. S34. Photoluminescence excitation (PLE) and emission spectra of a) $Sm(NO_3)_3.6H_2O$, b) $Eu(NO_3)_3.5H_2O$, c) $Tb(NO_3)_3.6H_2O$, d) $Dy(NO_3)_3.5H_2O$.

| Composite | Elements | ICP (wt%) |
|-----------|----------|-----------|
| **1:Eu** | $Cd^{2+}$: $Eu^{3+}$ | 13.25: 2.1 |
| **3:Eu** | $Zn^{2+}$: $Eu^{3+}$ | 5.54: 4.16 |
| **4:Eu** | $Cd^{2+}$: $Eu^{3+}$ | 10.88:2.15 |
| **5:Eu** | $Cd^{2+}$: $Eu^{3+}$ | 12.37:1.29 |

Table S4. ICP analysis for the samples (**X:Eu (X=1, 3, 4, 5)**) which had been immersed in 0.3 methanol solution containing nitrate salts of $Ln^{3+}$ cations for 3 days. The as-synthesized crystals of compound were used directly for post-modification without further treatment.

**References**

1    (a) Z. -B. Wang, H. -F. Zhu, M. Zhao, Y. -Z. Li, T. Okamura, W. -Y. Sun, H. -L. Chen, and N. Ueyama, *Crystal Growth & Design.*, 2006, **6**, 1420; (b) D. Bardelang, K. A. Udachin, D. M. Leek, J. C. Margeson, G. Chan, C. I. Ratcliffe, and J. A. Ripmeester, *Crystal Growth & Design*, 2011, **11**, 5598; (c) Z. B. Wang, M. Zhao, Y. Z. Li, H. –L. Chen, *Supramolecular Chemistry*, 2008, **20**, 689.

2    S. Lim, H. Kim, N. Selvapalam, K. J. Kim, S. J. Cho, G. Seo, and K. Kim, *Angew. Chem.*, 2008, **120**, 3400.

3    F. F. da Silva, C. A. F. de Oliveira, E. H. L. Falcão, J. Chojnacki, J. L. Neves, S. A. Jr, *Dalton Trans.*, 2014, **43**, 5435-5442.